Rigid waist shift: A new method for local coupling corrections in the LHC interaction regions

Felix Soubelet*
Physics Department, University of Liverpool, Liverpool L697ZE, United Kingdom and CERN, European Organization for Nuclear Research, Geneva CH-1211, Switzerland

Tobias Persson and Rogelio Tomás
CERN, European Organization for Nuclear Research, Geneva CH-1211, Switzerland

Oznur Apsimon† and Carsten P. Welsch
Physics Department, University of Liverpool, Liverpool L697ZE, United Kingdom and Cockcroft Institute, Warrington WA44AD, United Kingdom

(Received 20 January 2023; accepted 10 April 2023; published 16 May 2023)

Successful operation of large-scale particle accelerators depends on the precise correction of magnet field or alignment errors present in the machine. In the Large Hadron Collider (LHC), transverse linear coupling has been shown to have a significant impact on the beam dynamics. However, current measurement methods are not sufficient for precise local coupling measurement at the interaction point. In this paper, an approach to determine interaction region local coupling corrections with a rigid waist shift based on correlated global variables such as the closest tune approach $|C^-|$ is presented. The validity of the method is demonstrated through simulations and experimental measurements taken during the LHC Run 3 commissioning in 2022, where determined corrections were applied and led to a measured luminosity increase of 9.7% and 3.5% at the ATLAS and CMS detectors, respectively.

DOI: 10.1103/PhysRevAccelBeams.26.051001

I. INTRODUCTION AND MOTIVATIONS

Beam-based corrections of linear optics and nonlinear dynamics in colliders are essential for both beam control and in order to achieve the desired luminosity goals. The determination of corrections is based on measurements of global quantities—tune, chromaticity—or on local deviations from model values such as phase, β beating, or resonance driving terms (RDTs). The linear optics and coupling correction usually constitute the first phase of machine commissioning as both are major contributors to the performance of colliders and are required to be under good control for the next phases of commissioning. In the LHC, correction of linear coupling is based on the minimization of linear coupling RDTs [1].

The global effect of linear coupling in hadron colliders is quantified by the closest tune approach $\Delta Q_{\min}$, the minimum achievable distance between the fractional parts of the tunes [2]. To identify sources of coupling and determine corrections, in the LHC, the difference and sum coupling RDTs f_{1001} and f_{1010} are computed from turn-by-turn measurement data and compared to model values. The relation between coupling RDTs and the $\Delta Q_{\min}$ can be found in [1,3]. In recent years, significant efforts have been made to improve the measurement and correction of linear and nonlinear global coupling both in the LHC [4–13] and other synchrotrons [14–26], as its effect can lead to instabilities and unwanted dynamics in the machine [12,27–30]. Though global coupling may be well controlled, local variations of the coupling RDTs left after corrections have the potential to degrade target quantities, especially in complex machine segments such as collider insertion regions. For example, during the late 2018 ion run in the LHC, it was observed that while global coupling was well corrected, a local coupling bump around the ALICE detector had a significant impact on beam size and led to a reduction of the luminosity by up to 50% [31–33]. Figure 1 shows the expected beam size growth and luminosity decrease from various strengths of such a local coupling bump at the main experiments, highlighting the necessity of its proper handling for the LHC and High-Luminosity LHC (HL-LHC).

In the LHC local coupling correction is done by measuring the RDTs in the vicinity of the IP and using

*felix.soubelet@cern.ch
†Now at the University of Manchester.

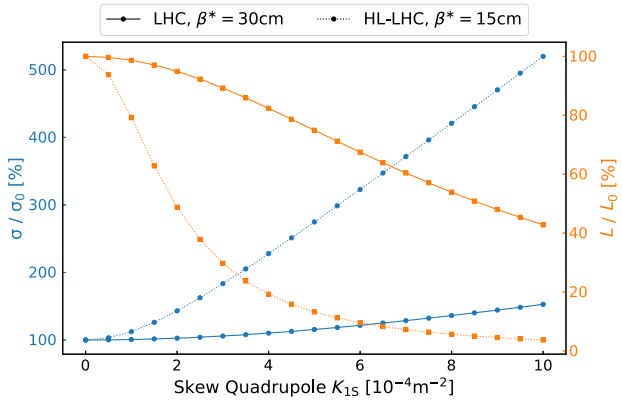

FIG. 1. Relative values of the rms beam size at IP1 (blue) as well as luminosity (orange) for different strengths of a local coupling bump around the IP made with skew quadrupoles, for the LHC and HL-LHC V1.5. Beam sizes are calculated according to Eq. (6) and luminosities according to Eq. (7). In the case of the HL-LHC, the relative beam size increase and subsequent luminosity loss are greater due to the larger β functions in the triplet.

two dedicated skew quadrupole correctors for compensation, based on a propagation done with the segment-by-segment (SbS) technique [34]. While the method is highly efficient for local phase corrections, it suffers inherent weaknesses making it not local enough for coupling corrections: unsuitable phase advances, an inability to disentangle the contributions of corrector magnets, and no information provided at the IP location.

In this paper, we present a new method that was developed—which breaks the degeneracy of the SbS technique—to determine the corrections of linear coupling at the interaction points, thus reducing beam sizes and hence improving the luminosity.

A brief introduction to the formalism and quantities of interest is given in Sec. II, followed by an explanation of the existing correction methods' limitations in Sec. III. The new method's concept along with simulations are exposed in Sec. IV, and experimental results from the LHC 2022 commissioning are presented in Sec. V. Finally, Sec. VI discusses the relevance of the method to other colliders.

II. RELEVANT THEORY

In the normal form formalism, the generating function of the transformation to normal form coordinates is the sum of various elements dictated by the f_{jklm} resonance driving terms [2,35–45]:

$$f_{jklm} = \frac{h_{jklm}}{1 - e^{i2\pi[(j-k)Q_x + (l-m)Q_y]}}, \tag{1}$$

where h_{jklm} is the Hamiltonian coefficient containing contributions from multipoles of order $n = j + k + l + m$, and Q_x, Q_y are, respectively, the horizontal and vertical tunes. The difference and sum resonance coupling RDTs, respectively, f_{1001} and f_{1010}, are reconstructed from turn-by-turn data measured at beam position monitors (BPMs) through the Courant-Snyder variable

$$h_{z,-} = \hat{z} - i\hat{p}_z, \qquad z \in \{x, y\}, \tag{2}$$

where $\hat{z}$ and $\hat{p}_z$ are normalized transverse position and momentum, respectively. As the momentum is not a directly measurable quantity with a BPM, it is reconstructed using two consecutive BPMs. The momentum at the nth BPM can be written as

$$\hat{p}_{z_n} = \frac{\hat{z}_{n+1} - \hat{z}_n \cos(\Delta\phi_z)}{\sin(\Delta\phi_z)}, \tag{3}$$

with $\Delta\phi_z$ the phase advance between the nth and $(n+1)$th BPM in the transverse z plane.

The closest tune approach, $\Delta Q_{\min}$, is a conventional measure of the global transverse coupling in a circular hadron machine. In the LHC, the fractional tunes (Q_x, Q_y) during the cycle are chosen close to the difference resonance [46] and as a consequence $|f_{1001}| \gg |f_{1010}|$ during normal operation. The $\Delta Q_{\min}$, also denoted $|C^-|$, is then related to the f_{1001} RDT through [1]:

$$|C^-| = \left| \frac{4\Delta}{2\pi R} \oint ds f_{1001} e^{-i(\phi_x - \phi_y) + is\Delta/R} \right|, \tag{4}$$

with Δ being the fractional tune separation between the uncoupled tunes.

In [47], the equations of motion are solved perturbatively under the influence of a weak skew quadrupole strength $j(s)$. Assuming that the machine is close to the difference coupling resonance $\Delta = Q_x - Q_y \to 0$, the $|C^-|$ can be approximated as

$$|C^-| = \frac{1}{2\pi} \left| \oint ds \sqrt{\beta_x(s)\beta_y(s)} j(s) e^{-i(\phi_x - \phi_y) + i\frac{s\Delta}{R}} \right|, \tag{5}$$

where s is the position around the ring, β_x and β_y are the horizontal and vertical β functions, ϕ_x and ϕ_y are the horizontal and vertical phase advances and R is the radius of the machine. These quantities are used throughout the presented studies and measurements.

In the presence of betatron coupling, usual Twiss parameters calculations in the formalism of Edwards and Teng [48] need to be adapted. One approach is to use the **C**-matrix [6] to do so but in these studies, the formalism of Ripken, developed in [49] and more accessible in [50,51] is used. It provides so-called Ripken parameters β_{kj}, α_{kj}, and γ_{kj}, where $k = 1 \ldots 3$ refers to the plane $(x, y, \ldots)$ and the index j refers to the eigenmodes, which are accurate in the presence of coupling. In the absence of coupling, it holds that $\beta_x = \beta_{11}, \beta_y = \beta_{22}$, and $\beta_{12} = \beta_{21} = 0$. In the coupled case, all β_N are nonzero and β_{11}, β_{22} are distinctively

different from β_x, β_y, respectively. The relations linking these quantities can be found in [52].

At the LHC IPs with round beams, the effect of the beam's tilt induced by betatron coupling [53] is negligible and its impact manifests as an increase in the beam size. In these studies, sizes were calculated from Ripken parameters according to [52]:

$$\langle z \rangle = \sqrt{\varepsilon_1 \beta_{1z} + \varepsilon_2 \beta_{2z}}, \qquad z \in \{x, y\}, \tag{6}$$

where ε_1 and ε_2 are the horizontal and vertical emittances, respectively. Figure 2 shows a reconstruction of transverse beam sizes at IP5 under varying the strength of a local coupling bump. While the beam ellipses show a $\gg 99\%$ overlap indicating a negligible tilt effect, the beam size in the most affected case is about 250% of the uncoupled case.

Instantaneous luminosities calculated for Fig. 1, in the absence of crossing angles, are done so according to [54]:

$$\mathcal{L} = \frac{N_1 N_2 f_{\mathrm{rev}} N_b}{2\pi \sqrt{(\sigma_{x,1}^2 + \sigma_{x,2}^2)} \sqrt{(\sigma_{y,1}^2 + \sigma_{y,2}^2)}}, \tag{7}$$

where N_n is the number of protons per bunch in beam n, f_{rev} the revolution frequency of particles, N_b the number of bunches per beam, and $\sigma_{z,n}$ is the size at the IP of beam n in the transverse plane z, calculated according to Eq. (6).

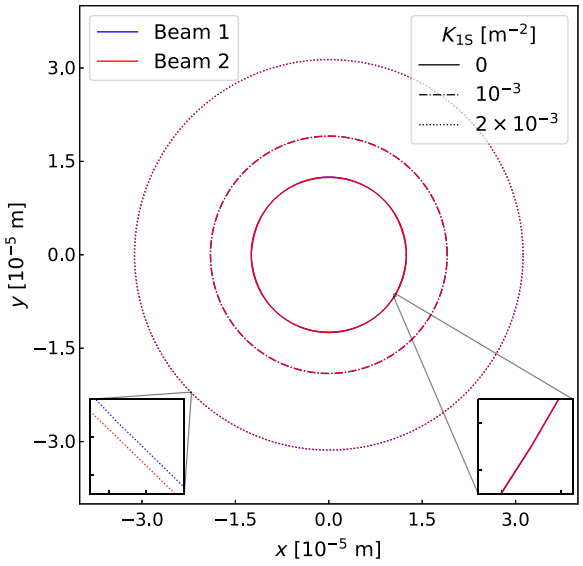

FIG. 2. Transverse beam sizes at the IP5 location at 6.8 TeV and $\beta^* = 30$ cm with normalized emittances $\varepsilon_x = \varepsilon_y = 3.75$ μm, for different strengths of a local coupling bump around the IP made with skew quadrupoles. The ellipses are reconstructed through the σ_{11}, σ_{13}, and σ_{33} terms of the sigma matrix.

III. CURRENT CORRECTION METHODS AND THEIR LIMITATIONS

The approach to local coupling correction in the LHC has been to use the segment-by-segment technique [34] to calculate the powering of the skew quadrupole correctors left and right of the IP. The IR around IP1—the ATLAS detector—is shown in Fig. 3, where the position of the dedicated correctors is highlighted in green.

A more detailed view of the corrector package for the LHC experimental insertions is shown in Fig. 4, where the dedicated skew quadrupole (a2 order) correctors are in the blue block C2 located right before triplet quadrupole Q3, on the IP side. In Table I, one can find the definition of the colinearity knob, a powering setting convention for the skew quadrupole correctors—the MQSX magnets—which

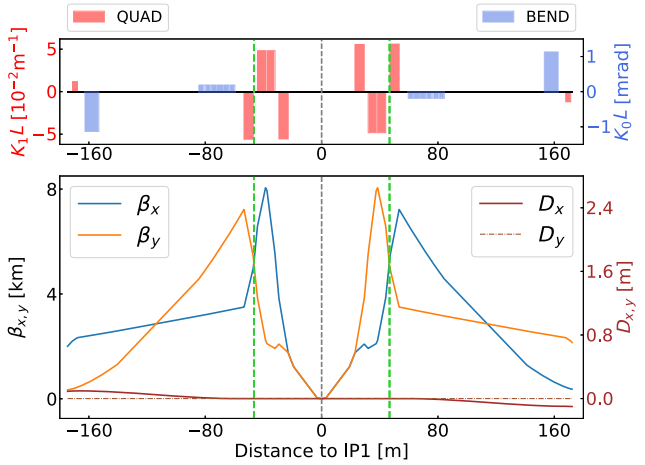

FIG. 3. LHC IR1 for a round optics configuration at 6.8 TeV and $\beta^* = 30$ cm. The upper plot shows the machine layout with dipoles in blue and quadrupoles in red. The lower plot shows β and dispersion functions for both transverse planes. The vertical green lines highlight the location of the skew quadrupole correctors used for corrections.

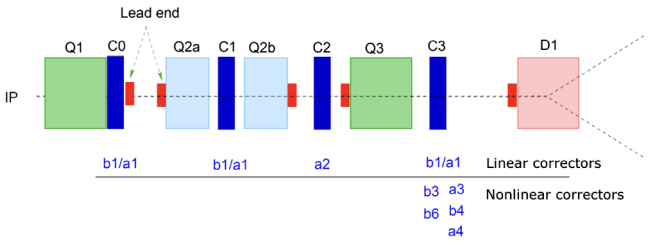

FIG. 4. Layout of the triplet magnets and the linear and nonlinear correctors in the LHC experimental insertions [56], showing common aperture magnets. The Q1, Q2a/b, and Q3 are triplet quadrupoles while the C0, C1, C2, and C3 are corrector packages with the field order indicated below. D1 is the separation dipole, diverging Beam 1 and Beam 2 to their respective beamlines. The skew quadrupole correctors correspond to order a2 and are located in the C2 package.

TABLE I. Definition of one unit of the colinearity knob, a powering setting of the IR skew quadrupole correctors.

Magnet	K_{1S} [m^{-2}]
MQSX.3R[IP] $\rightarrow K_{1S}$	$+10^{-4}$
MQSX.3L[IP] $\rightarrow K_{1S}$	-10^{-4}

was originally designed for a flat optics experiment [55] and acts antisymmetrically on the powering of the left and right corrector magnets. Since for round optics, the β functions are by design identical at the correctors and given the $\sim 180°$ phase advance between the two magnets, assuming a good enough β beating correction, the knob does not impact the global coupling while inducing a closed coupling bump around the IP.

The SbS technique treats a segment of the accelerator as an independent line and propagates measured optics properties through this segment using the MAD-X code [57]. One then tries to find correction settings—powering changes of selected magnets—that would best reproduce the propagated optics. Thereby, inverting these settings and applying the inverted values in the machine corrects the measured errors. Coupling corrections calculated with the SbS technique mostly aim to compensate for the coupling coming from the IR. These corrections are essential in commissioning in order to reach low β^* with good optics control: at $\beta^* = 30$ cm, the local errors compensated in Run 2 [33] would contribute to the $|C^-|$ by the amount of 0.33—too high for the arc correctors to handle.

However, due to unfavorable phase advances in between BPMs in the IRs, it is difficult to get a good measurement of the coupling RDTs in these regions. When looking at Eq. (3) and knowing that the phase advance in the IR is ~ 0 from BPM to BPM, and $\sim \pi$ from one side of the IP to the other, one can see why the reconstruction of the momentum and later on the coupling RDTs is very difficult at BPMs around the IP. Figure 5 shows the coupling RDTs propagated with the SbS technique in the IR1 segment, from measurements taken during the LHC 2021 beam tests and 2022 commissioning. Large error bars can be noticed, and while no given case appears specifically better than the other, the orange line corresponds to a better correction.

Furthermore, the SbS technique does not allow one to differentiate the contribution of one individual corrector from the other, making it difficult to find the correct balance of left and right powering settings: as both correctors can compensate each other one might find a good compensation of the overall IR contribution to global coupling which also deteriorates the coupling situation at the IP. Additionally, the method cannot provide a measurement for operators to estimate the coupling at IP, as there are no BPMs at the location.

The usual technique to get a measurement of β functions at the IP is K-modulation [58,59]. However, it has been shown that K-modulation measurements are robust against the presence of local coupling, both analytically [60,61] and experimentally [62], preventing the possibility of directly measuring the beam size variation at an IP from the local coupling.

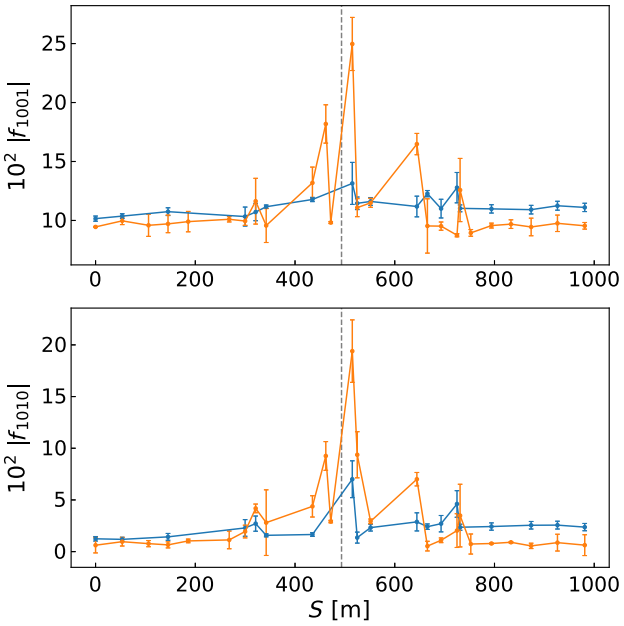

FIG. 5. Propagation of the measured $|f_{1001}|$ and $|f_{1010}|$ for beam 1 around IP1, measured with two different corrector settings. The orange line corresponds to a -4 trim of the colinearity knob compared to the blue line and leads to a beam size smaller by 9.2%.

In order to be able to correct the coupling in the IRs—and more specifically at the IP—during commissioning with low intensity pilot beams, a new method complementary to SbS is needed. Section IV presents the concept of such a method.

IV. RIGID WAIST SHIFT FOR LOCAL COUPLING CORRECTION

In order to circumvent the issues related to measuring the local coupling at the IP, it became necessary to find a way to relate it to other measurable quantities.

A. Concept and simulations

In order to do so, the idea is to apply a rigid waist shift (RWS) to the beam—meaning all four betatron waists moving simultaneously—in order to break the (anti-) symmetry of the optics in the IR. An RWS can be achieved by unbalancing the strength of the triplet quadrupoles on either side of the IP, antisymmetrically. Table II gives the definition of the RWS knob used to achieve this goal. Making away with the symmetry allows to break the locality of a coupling bump, making the impact of even truly local coupling errors measurable everywhere.

TABLE II. Definition of one unit of the rigid waist shift knob, acting on the powering of triplet quadrupoles (KQX) left and right of the IP.

Circuit	Powering Δ
KQX.R[IP]	−0.5%
KQX.L[IP]	0.5%

However, this simple implementation of the RWS has a strong effect on the optics across the machine. For instance, simulations show that its application causes a 15% deviation from the achieved $|C^-|$ to the target value set through the LHC coupling knob. The RWS is also expected to lead to a 20%–30% increase in β beating in the machine, depending on the observed plane. These optics deviations will change the impact of probed errors, namely the skew quadrupolar impact on the $|C^-|$. In order to limit this impact on the optics, a new correction knob has been developed that also makes use of the individually powered quadrupoles Q4 to Q10 (included) to tune the optics functions and rematch them at the edges of the IR. This rematching was done with the MAD-X code and a specifically made PYTHON package [63].

Figure 6 shows the coupling RDTs from a closed coupling bump created through the colinearity knob in the presence and absence of an RWS. When applying the waist shift and breaking the optics symmetry in the IR, one can observe a leakage of the RDTs outside the limits of the coupling bump. These RDTs will then have a residual presence in the machine, which can be measured and reconstructed from turn-by-turn data from BPMs with more suitable phase advances.

In the case of only skew quadrupolar coupling sources, Eq. (5) becomes a summation of the individual sources and the $j(s)$ term becomes J_w—the integrated skew quadrupole strength of the source indexed by w—in that summation,

$$|C^-| = \left| \frac{1}{2\pi} \sum_w \sqrt{\beta_x^w \beta_y^w}\, J_w e^{-i(\phi_x - \phi_y) + i\frac{s\Delta}{R}} \right| = \left| \frac{1}{2\pi} \sum_w \sqrt{\beta_x^w \beta_y^w}\, J_w e^{-i(\phi_x - \phi_y)} \right| + O(\Delta). \quad (8)$$

Taking into account the phase advances between the two contributing corrector magnets, the contribution to the global coupling can be written as

$$\Delta C^- = \frac{1}{2\pi} \sum_w \sqrt{\beta_x^w \beta_y^w}\, J_w = \frac{1}{2\pi} \left(\sqrt{\beta_x^l \beta_y^l} k_S^l L + \sqrt{\beta_x^r \beta_y^r} k_S^r L \right), \quad (9)$$

with $k_S^w L = J_w$ the integrated strength of the skew quadrupole at position w, and l and r superscripts denoting the corrector left or right of the IP, respectively. From the symmetry of the optics in the IR as seen in Fig. 3, and with identical lengths and opposite powering settings as seen in Table I, this reduces to 0. When applying an RWS, the $\sqrt{\beta_x \beta_y}$ terms and the phase advances change enough that the contribution to global coupling becomes nonzero.

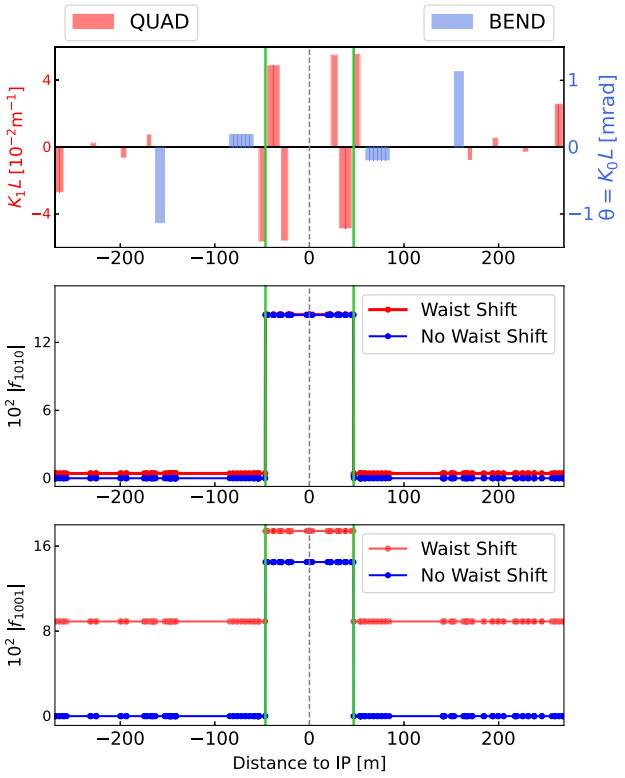

FIG. 6. Linear coupling RDTs in the vicinity of IP1 under a coupling bump, with and without an RWS. The vertical green lines represent the positions of the skew quadrupole correctors used to implement the coupling bump. A colinearity knob setting of 10 and a rigidity waist shift knob setting of 1 were used, which results in a 0.5% change in the triplet powering knob and a 43.5 cm shift of the beam waists at $\beta^* = 30$ cm.

As a consequence, under an RWS a local coupling bump will have a direct impact on the global coupling, measured as the $|C^-|$. This is shown in Fig. 7, where changes in the setting of the colinearity knob now have a strong effect on the $|C^-|$. The behavior seen in Fig. 7, though theoretical, has been tested in the machine [62].

This behavior opens the possibility of using an RWS to probe IR local coupling through the measured global coupling. Simulations have been done with the MAD-X code to investigate the feasibility of finding local coupling correction settings using an RWS. For the conducted studies, the LHC Run 3 lattice [64] and $\beta^* = 30$ cm optics were used and the IRs around LHC points 1 (ATLAS) and 5 (CMS) were considered. A local coupling bump was created by introducing identical tilt errors in triplet quadrupoles Q3—thus giving a skew quadrupolar component—and compensation was done by acting on the setting of the

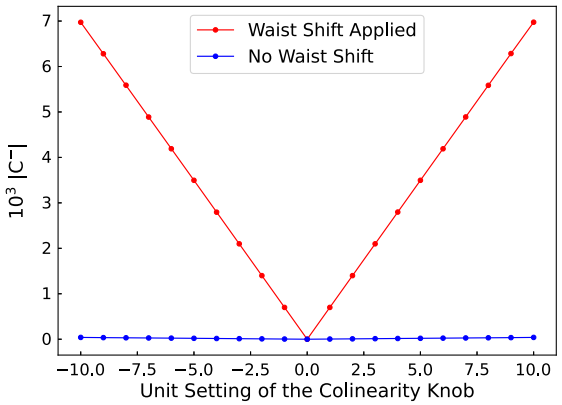

FIG. 7. Impact of the colinearity knob on the global $|C^-|$, calculated according to Eq. (4), with and without applying an RWS.

colinearity knob. Figure 8 shows the values of the resulting $|C^-|$ across the parameter space when an RWS is applied.

Figure 9 shows the resulting beam size increase as a ratio to the nominal beam size across the same parameter space, highlighting that minimization of the growth is possible though a wrong setting would enhance the phenomenon.

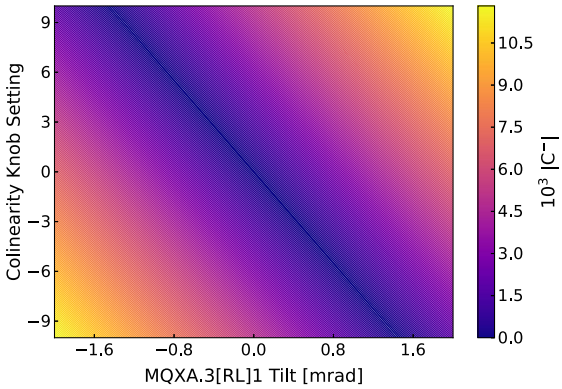

FIG. 8. Resulting $|C^-|$ [Eq. (4)] for various combinations of tilt error and colinearity knob settings, when applying an RWS.

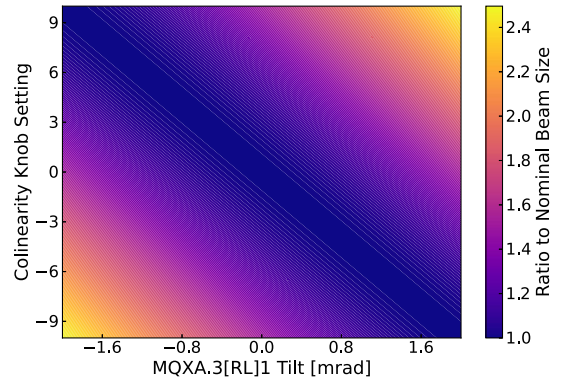

FIG. 9. Resulting beam size [Eq. (6)] increase for identical settings of tilt error and colinearity knob settings as Fig. 8 but without an RWS.

Simulations replicating more complex scenarios akin to operational conditions were performed. The simulations were run in MAD-X with the LHC 2022 lattice [64] and $\beta^* = 30$ cm optics. Tilt errors were introduced in the triplet quadrupoles Q3 around IP1 as mentioned above to create a closed local coupling bump. Additionally, tilt errors were added to an individually powered quadrupole in IR5 (for instance Q5) to include the presence of expected residual local coupling errors in the other main IP, which contributes to the global coupling by the amount of 10^{-3}. Some global coupling sources are also added with a dedicated knob [65] that bring the global coupling to 10^{-2}, which is then corrected through a routine, bringing it down to 3×10^{-3}, a level similar to what is achieved in the machine [66,67]. The RWS and colinearity knobs were then powered to different settings, and the resulting $|C^-|$ and IP beam sizes were determined in all settings combinations.

Similar to studies made in Figs. 8 and 9, an entire parameter space of implemented errors and corrections has been explored. The evolution of both the $|C^-|$ under an RWS and the beam size growth at IP1 without an RWS for one of these simulations can be seen in Fig. 10.

It can be observed that settings minimizing the measured $|C^-|$ under an RWS are close to minimizing the local coupling and beam size increase without said RWS. In this case, these settings compensate also the contribution of the other added sources to the global coupling, on top of the local ones. Similarly to previous studies a great correlation is observed, and across the parameter space one computes a 0.96 Pearson correlation coefficient between the two quantities shown in Fig. 10. This confirms the link

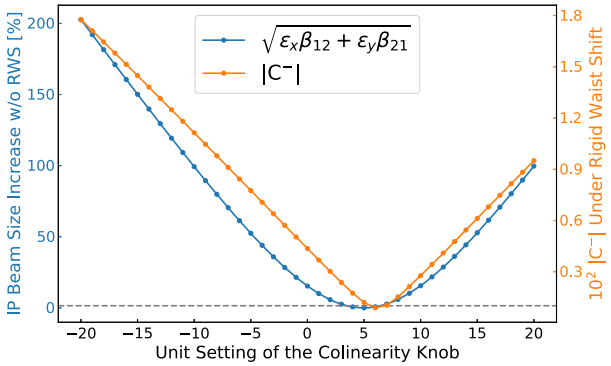

FIG. 10. Resulting $|C^-|$ [Eq. (4)] under RWS and IP1 beam size [Eq. (6)] without RWS relative to the nominal scenario, for various powering of the skew quadrupole correctors, after introducing a 1-mrad tilt error on the Q3s left and right of IP1, a 0.5-mrad tilt error in the Q5 right of IP5 and some global coupling sources (coupling knob at 10^{-2}). The black dotted line represents the threshold of a 1% beam size increase from the nominal scenario.

between the measured $|C^-|$ and quantities of interest at the IP location: thanks to the RWS the local coupling and its effect on beam size can be related to and probed via the measured $|C^-|$.

B. Determining corrections

The corrections that would compensate only the local sources are determined by comparing the measured $|C^-|$ to simulations, such as the orange line in Fig. 10. In the real machine, some coupling will remain in the arcs due to a nonperfect global correction and nonlocal SbS corrections. As the method probes local errors' impact through the $|C^-|$, it will naturally be sensitive to the global coupling in the machine, which should be replicated: simulations need to include a model of the global coupling from the measured machine. Although the overall behavior of simulations remains similar when including this component, an important change from the line seen in Fig. 10 is the location of the setting that minimizes the $|C^-|$. The relevance of this property will be discussed below.

The reproduction of the machine's global coupling in simulations becomes necessary as soon as strong non-IR sources are present and can be done in different ways. In studies, various implementations were tested: random tilts in all quadrupoles, LHC-specific knobs [65], longitudinal misalignment of sextupoles, field errors in specific magnets, or random combinations of the above. It was found that to the levels of coupling we achieve after correcting the machine, the distribution and implementation of sources had little impact on the minimization point of the $|C^-|$ curve under an RWS, as long as the overall pattern of the f_{1001} and the level of coupling measured in the machine were accurately reproduced. As a consequence, in simulations this reproduction was done by including the coupling correction knobs implemented in the machine, as determined during earlier commissioning steps.

By comparing measurements from a colinearity knob scan to simulations—where the former includes the impact of local errors, but the latter assumes no local errors—one can single out the contribution of the local sources to the global coupling. Figure 11 shows the resulting $|C^-|$ values under an RWS during a colinearity knob scan, for one of the simulation scenarios mentioned previously (Fig. 10), and a similar scenario in which no local coupling sources were implemented in IR1. The former represents what would be measured in the machine, including the contribution of local sources, while the latter represents the simulations to compare such a measurement to, which include all contributions to global coupling except for the IR local sources.

Applying a trim of the colinearity knob setting linearly translates the curves of Fig. 11 horizontally. This behavior is valid and verifiable in both simulation and measurements. Therefore, one looks to determine a colinearity knob trim that, if applied in the machine, would bring the

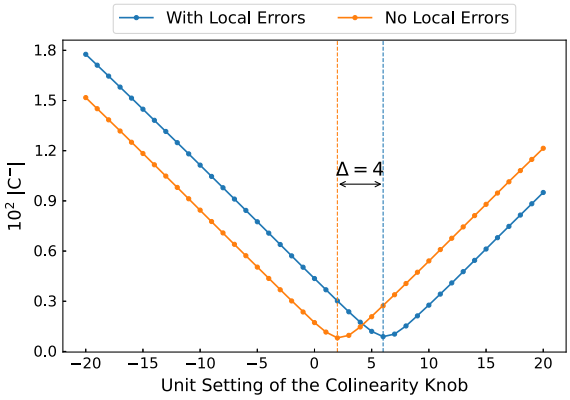

FIG. 11. Resulting $|C^-|$ in simulations as done for Fig. 10, with (blue) and without (orange) local coupling sources in IR1. The former is representative of the effects included in a machine measurement, while the latter is representative of simulations to compare such measurements to.

measurement's $|C^-|$ minimization point to that of the simulation. As this difference if fully explained by local sources, this trim contains the information on the local error in terms of colinearity knob setting: powering of the corrector magnets. In Fig. 11, the minima are highlighted with vertical lines and the aforementioned correction trim is determined from the relative position of these two minima. The value is different from that of the minimization in Fig. 10 as there global sources are also compensated while this correction aims at compensating only the local sources.

When only considering the local sources used for the results in Fig. 11 and inputting the correction trim suggested, one obtains a good compensation of the beam sizes at IP1. Figure 12 shows the impact of these local errors and the effect of applying the suggested correction trim. The exactitude and effectiveness of the determined correction can be improved by performing more granular scans of the

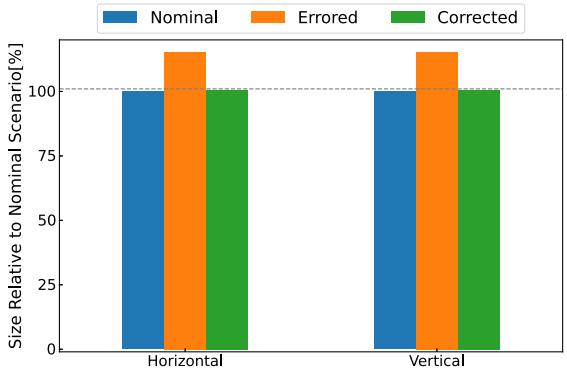

FIG. 12. Relative IP beam sizes when compared to the nominal scenario (blue) when inputting the local errors used in the study for Fig. 11 (orange) and after applying the suggested correction (green). The black dotted line represents the threshold of a 1% beam size increase from the nominal scenario.

colinearity knob, but the values used are representative of what can be done in measurements.

C. Rigid waist shift procedure

The correction procedure for local linear coupling is then made of three steps. First, calculating and applying a correction of the IR contribution to global coupling based on RDTs from turn-by-turn measurements, using the SbS technique. Second, breaking the optics symmetry between the right- and left-hand side of the IP by applying an RWS and performing a scan of the colinearity knob. Finally, analyzing the measurement data and comparing it to simulations in order to find a colinearity knob adjustment setting that minimizes the global coupling, without impacting the correction found in step 1.

These measurements can be performed for each IR and for each beam, and the subsequent determined corrections can then be directly applied to the machine.

V. EXPERIMENTAL RESULTS

A first set of local coupling corrections were determined during the LHC 2021 beam tests and 2022 commissioning using the SbS technique. The RWS method was then implemented in both IR1 and IR5 at 6.8 TeV and $\beta^* = 30$ cm to determine final correction settings in the form of adjustments from the SbS corrections. Figure 13 shows the additional β beating induced across the machine for beam 1 from applying the RWS in IR5, before and after the application of the optics rematching knob. The β functions in these measurements are reconstructed according to [68].

The measured impact is in agreement with what was expected from earlier simulations, leading to a 15%–25% additional β beating in the machine depending on the observed beam and plane; while the rematching knob brought this beating back to about 5% where it was previously kept thanks to existing corrections. This showcases the great efficiency of the optics rematching knob. Naturally, some strong deviations are noticed close to IP5 (going out of range of the y axis) as the optics, there are changed on purpose, but also because β functions reconstruction close to the IPs is of relatively low quality.

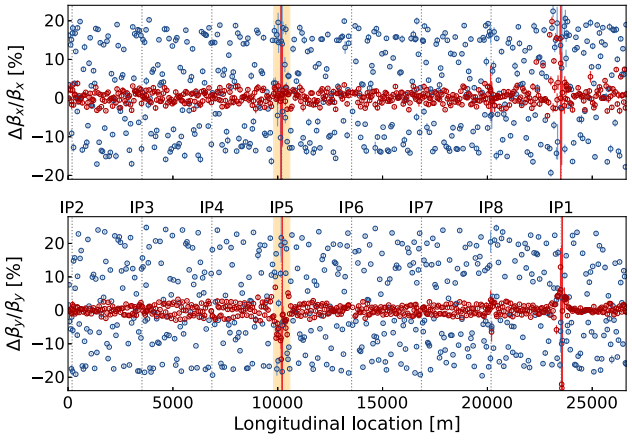

FIG. 13. The beam 1 additional β beating observed in the machine from the implementation of the RWS in IR5 at 6.8 TeV and $\beta^* = 30$ cm, using only triplet quadrupoles (blue) and with the optics rematching using all quadrupoles in the IR (red). The highlighted area (orange) shows where magnetic elements are affected by the knobs.

With the waist shift in the machine, scans of the colinearity knob (Table I) were performed. At each setting, a few measurements were taken by method of beam excitation, from which the coupling RDTs were computed. As the optics are affected—and rematched—differently for beam 1 and beam 2, a scan of the colinearity knob is performed for each beam and for each IR. Different scans were done with different granularity due to time constraints.

For each measurement, the RDTs across the machine are normalized to the base case with the RWS applied, global coupling corrected and no colinearity knob trim; and only then the $|C^-|$ is computed according to Eq. (4). This way, only the variations due to the changes of the colinearity knob are visualized and compared to simulations. In said simulations, the global coupling of the machine is reproduced by introducing the coupling correction knobs implemented in the machine.

In Figs. 14 and 15, comparisons are shown between scan measurements and simulations for IR1 beam 2 and beam 1, respectively. Measurements at IR5 are not shown for brevity but are compiled in the table below. The delta between minimization settings, corresponding to the suggested adjustment, is highlighted on each plot. The relatively low range of values is due to the aforementioned RDTs normalization, and the different

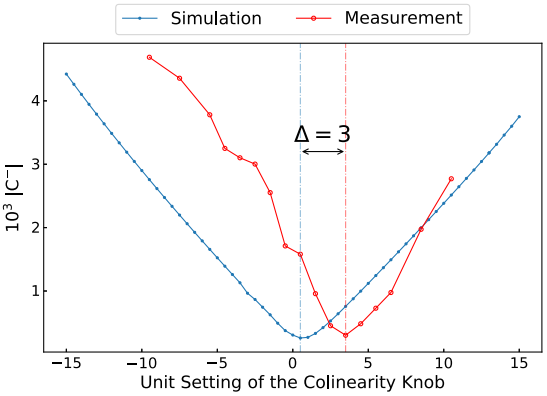

FIG. 14. Measurement scan done at IR1 for beam 2 and simulations for the same setup. The minima of both curves are highlighted by vertical dashed lines and the delta between the two, suggesting the remaining error to correct, is displayed on the graph.

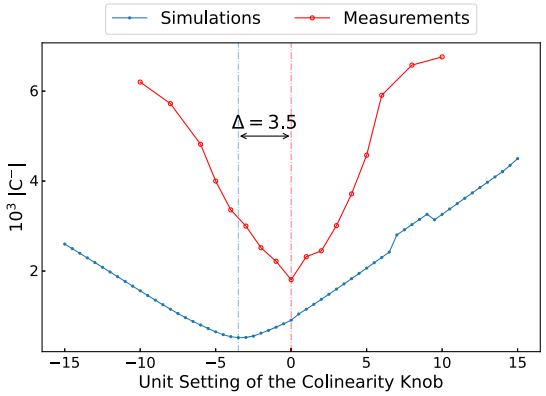

FIG. 15. Measurement scan done at IR1 for beam 1 and simulations for the same setup. The minima of both curves are highlighted by vertical dashed lines and the delta between the two, suggesting the remaining error to correct, is displayed on the graph.

behavior of beam 1 and beam 2 simulations is explained by the different coupling situation in each beam: throughout commissioning, beam 2 has showcased little natural coupling while beam 1 required significantly stronger global coupling corrections.

Simulations for beam 2 suggest that the reproduced global coupling has little effect on the procedure, and the colinearity knob scan could almost be used alone to determine the corrections. For beam 1 simulations, however, the impact of the reproduced global coupling appears much more substantial, as was the case in the machine, and these highlight the need to compare the scan measurements to simulations. Overall, this comparison is needed in the case that there are significant coupling errors in the arcs. It is worth noting that both beams' measurements converge to similar correction suggestions.

TABLE III. Correction adjustments suggested by rigid waist shift scans, on top of the existing segment-by-segment corrections that were in the machine.

	Suggested Δk [10^{-4} m^{-2}]	
Scan	Beam 1	Beam 2
IR1	−3.5	−3
IR5	−2	−1.5

TABLE IV. Luminosity gains observed at the main experiments ATLAS and CMS from the method's suggested corrections.

	Luminosity gain (%)	
Experiment	$\beta^* = 30$ cm	$\beta^* = 42$ cm
ATLAS (IP1)	9.7	5.2
CMS (IP5)	3.5	1.5

Table III shows a summary of the suggested correction settings for each beam and IR. While slightly different corrections are suggested from independent measurements of beam 1 and beam 2, it is possible that both values are simultaneously true. While most of the error contribution is expected to come from the dual-beam triplet quadrupoles and be common to both beams, errors in double aperture magnets Q4 to Q10 would affect each beam individually. Furthermore, the orbit and hence feed-down but also the β ratio between sources and correctors are different for both beams.

The suggested adjustments were applied, and their impact was assessed based on instantaneous luminosity measurements. Figure 16 shows the performed trims and subsequent measured luminosity changes at IP1. The instantaneous luminosity signal slightly trails up after the end of the correction adjustment trim as the ATLAS experiment publishes a time-averaged value. Similar trims were done in both IR1 and IR5 at $\beta^* = 30$ cm and $\beta^* = 42$ cm.

For each measurement, values around the suggested adjustment were also tested in order to look for the best local setting. Table IV gives a summary of the observed luminosity improvements for each performed trim.

It is expected to observe lower gains at a higher β^* since the $\sqrt{\beta_x \beta_y}$ term of Eq. (5) is substantially lower in the triplets for the less squeezed optics. It is also expected to notice a lower improvement at the CMS detector based on the numbers in Table III: a lower suggested adjustment indicates a smaller coupling error remains in IR5 than in IR1, and the subsequent smaller applied correction recovers less luminosity.

The adjustments determined with the RWS have been incorporated into the nominal corrector settings and the LHC now uses the resulting skew quadrupole powerings in normal operation.

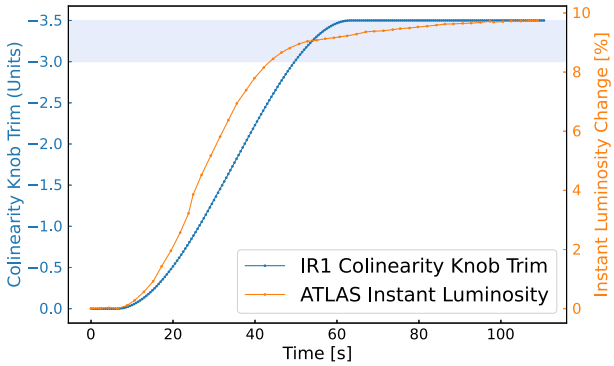

FIG. 16. Trim of the colinearity knob setting (blue) and observed IP1 instantaneous luminosity change (orange) at 6.8 Tev and $\beta^* = 30$ cm. The blue area highlights the trim values suggested by the RWS method, which varies for beam 1 and beam 2.

VI. RELEVANCE TO OTHER COLLIDERS

For any collider, the requirement of small β functions for collisions is a key design parameter and leads to using a doublet or triplet of quadrupoles to achieve the necessary intense focusing of the beams at the IP. On either side of the collision point, in the drift space leading to the first quadrupole, the β functions evolve as

$$\beta(s) = \beta^* + \frac{s^2}{\beta^*}, \tag{10}$$

where β^* is the β function at the IP and s denotes the distance from the IP. Using L^* as the length of this drift space, the phase advance from IP point to said quadrupole is

$$\mu = \int_0^{L^*} \frac{1}{\beta(s)} ds = \int_0^{L^*} \frac{\beta^*}{\beta^{*2} + s^2} ds, \tag{11}$$

which one can integrate to obtain

$$\mu = \beta^* \left[\frac{1}{\beta^*} \tan^{-1}\left(\frac{s}{\beta^*}\right) \right]_0^{L^*} = \tan^{-1}\left(\frac{L^*}{\beta^*}\right). \tag{12}$$

Then, for traditionally $L^* \gg \beta^*$, one gets

$$\mu \simeq \tan^{-1}(\infty) \simeq \frac{\pi}{2}. \tag{13}$$

As a consequence, for a typical collider layout, the phase advance from left to right doublet/triplet quadrupoles is $\sim\pi$ and tilts in said quadrupoles are susceptible to create a coupling bump around the IP.

Furthermore, SbS limitations encountered in the LHC would also be present: no observation point at the IP, and due to the large β functions in these quadrupoles, the phase advance from element to element close to the IP is very close to 0, making the accurate reconstruction of coupling RDTs difficult [see Eq. (3)].

These conditions were confirmed in existing and future machines: the High Luminosity LHC and FCC-hh lattices being based on the LHC's, they share the same issues. The FCC-ee [69] V22 lattice was used in simulations to confirm these conditions and the possibility of a close coupling bump from doublet tilts. Another existing machine, SuperKEKB, has also encountered nontrivial issues with local coupling in its High Energy Ring [70].

For the aforementioned accelerators but also more generally for most circular collider layouts, the presented use of an RWS could provide a useful method to tackle local linear coupling.

VII. CONCLUSIONS

A good correction of the local coupling in the LHC IRs is essential to ensure the design beam size at IPs. The existing correction methods, while crucial for safe machine operation and squeezing of the beams, do not provide an accurate way to determine correction settings of the coupling inside the IRs and specifically at the IP locations.

In this article, we have presented a newly developed method to determine these correction settings which relies on the application of a rigid waist shift and a necessary rematching of the optics. The method was implemented during the LHC 2022 commissioning, and corrections were successfully determined from beam-based measurements. These corrections were applied in the machine and confirmed through luminosity measurements, leading to substantial instantaneous luminosity gains.

This new method allows us to determine corrections early on in commissioning with low intensity beams and without requiring a collimation setup for luminosity scans. Furthermore, it enables distinguishing between the two beams, which could require different types of adjustments: magnet realignment, orbit corrections, etc.

This new method is of relevance for colliders where the local coupling is of concern, such as the High Luminosity LHC, SuperKEKB, or FCC-ee.

ACKNOWLEDGMENTS

We greatly thank all LHC Machine Coordinators, Engineers In Charge, and the operation crew for their continuous support during the optics commissioning. The authors also would like to thank the Optics Measurements and Corrections team members for their continued valuable feedback and fruitful discussions. The use of various open-source software [57,71–79] in the presented studies is also acknowledged. This work was supported by the STFC Liverpool Centre for Doctoral Training on Data Intensive Science (LIV.DAT) under Grant Agreement No. ST/P006752/1.

[1] T. Persson and R. Tomás, Improved control of the betatron coupling in the Large Hadron Collider, Phys. Rev. ST Accel. Beams **17**, 051004 (2014).

[2] G. Guignard, The general theory of all sum and difference resonances in a three-dimensional magnetic field in a synchrotron, CERN, Geneva, Technical Report No. CERN-ISR-MA/75-35, 1975.

[3] E. J. Hoydalsvik, T. H. B. Persson, and R. Tomas Garcia, Evaluation of the closest tune approach and its MAD-X implementation, CERN, Geneva, Technical Report No. CERN-ACC-NOTE-2021-0022, 2021.

[4] R. Tomás, M. Aiba, A. Franchi, and U. Iriso, Review of linear optics measurement and correction for charged particle accelerators, Phys. Rev. ST Accel. Beams **20**, 054801 (2017).

[5] R. Miyamoto, R. Calaga, M. Aiba, R. Tomás, and G. Vanbavinckhove, Measurement of coupling resonance driving terms in the LHC with AC dipoles, in *Proceedings of 2nd*

International Particle Accelerator Conference, IPAC'11, San Sebastián, Spain (JACoW, Geneva, Switzerland, 2011).

[6] R. Calaga, R. Tomás, and A. Franchi, Betatron coupling: Merging Hamiltonian and matrix approaches, Phys. Rev. ST Accel. Beams **8**, 034001 (2005).

[7] E. H. Maclean, R. Tomás, M. Giovannozzi, and T. H. B. Persson, First measurement and correction of nonlinear errors in the experimental insertions of the CERN Large Hadron Collider, Phys. Rev. ST Accel. Beams **18**, 121002 (2015).

[8] E. H. Maclean, R. Tomás, F. S. Carlier, M. S. Camillocci, J. W. Dilly, J. Coello de Portugal, E. Fol, K. Fuchsberger, A. Garcia-Tabares Valdivieso, M. Giovannozzi, M. Hofer, L. Malina, T. H. B. Persson, P. K. Skowronski, and A. Wegscheider, New approach to LHC optics commissioning for the nonlinear era, Phys. Rev. Accel. Beams **22**, 061004 (2019).

[9] T. H. B. Persson, Y. Inntjore Levinsen, R. Tomás, and E. H. Maclean, Chromatic coupling correction in the Large Hadron Collider, Phys. Rev. ST Accel. Beams **16**, 081003 (2013).

[10] R. Tomás, T. H. B. Persson, and E. H. Maclean, Amplitude dependent closest tune approach, Phys. Rev. Accel. Beams **19**, 071003 (2016).

[11] E. Maclean, T. Persson, and R. Tomás, Amplitude dependent closest tune approach generated by normal and skew octupoles, in *Proceedings of 8th International Particle Accelerator Conference, IPAC-2017, Copenhagen, Denmark* (JACoW, Geneva, Switzerland, 2017), pp. 3147–3150, 10.18429/JACoW-IPAC2017-WEPIK091.

[12] N. Biancacci and R. Tomás, Using ac dipoles to localize sources of beam coupling impedance, Phys. Rev. Accel. Beams **19**, 054001 (2016).

[13] E. H. Maclean, F. S. Carlier, S. Fartoukh, T. H. B. Persson, P. K. Skowronski, R. Tomas Garcia, and D. A. Wierichs, Demonstration of coupling correction below the per-mil limit in the LHC, CERN Technical Report No. CERN-ACC-NOTE-2016-0053, 2016.

[14] K. Tian, J. Safranek, and Y. Yan, Machine based optimization using genetic algorithms in a storage ring, Phys. Rev. ST Accel. Beams **17**, 020703 (2014).

[15] Y. Ohnishi, K. Ohmi, H. Koiso, M. Masuzawa, A. Morita, K. Mori, K. Oide, Y. Seimiya, and D. Zhou, Measurement of chromatic $x - y$ coupling, Phys. Rev. ST Accel. Beams **12**, 091002 (2009).

[16] M. Carlà, G. Benedetti, T. Günzel, U. Iriso, and Z. Martí, Local transverse coupling impedance measurements in a synchrotron light source from turn-by-turn acquisitions, Phys. Rev. Accel. Beams **19**, 121002 (2016).

[17] X. Shen, S. Y. Lee, M. Bai, S. White, G. Robert-Demolaize, Y. Luo, A. Marusic, and R. Tomás, Application of independent component analysis to ac dipole based optics measurement and correction at the relativistic heavy ion collider, Phys. Rev. ST Accel. Beams **16**, 111001 (2013).

[18] D. Sagan, R. Meller, R. Littauer, and D. Rubin, Betatron phase and coupling measurements at the Cornell electron/positron storage ring, Phys. Rev. ST Accel. Beams **3**, 092801 (2000).

[19] W. Fischer, Robust linear coupling correction with N-turn maps, Phys. Rev. ST Accel. Beams **6**, 062801 (2003).

[20] A. Franchi, Error analysis of linear optics measurements via turn-by-turn beam position data in circular accelerators, arXiv:1603.00281.

[21] R. Tomás, M. Bai, R. Calaga, W. Fischer, A. Franchi, and G. Rumolo, Measurement of global and local resonance terms, Phys. Rev. ST Accel. Beams **8**, 024001 (2005).

[22] X. Yang and X. Huang, A method for simultaneous linear optics and coupling correction for storage rings with turn-by-turn beam position monitor data, Nucl. Instrum. Methods Phys. Res., Sect. A **828**, 97 (2016).

[23] X. Huang, J. Corbett, J. Safranek, and J. Wu, An algorithm for online optimization of accelerators, Nucl. Instrum. Methods Phys. Res., Sect. A **726**, 77 (2013).

[24] E. C. Raka, Measurement of the linear coupling in the Brookhaven AGS, IEEE Trans. Nucl. Sci. **22**, 1938 (1975).

[25] A. Franchi, L. Farvacque, J. Chavanne, F. Ewald, B. Nash, K. Scheidt, and R. Tomás, Vertical emittance reduction and preservation in electron storage rings via resonance driving terms correction, Phys. Rev. ST Accel. Beams (2011).

[26] M. Aiba, M. Böge, N. Milas, and A. Streun, Ultra low vertical emittance at SLS through systematic and random optimization, Nucl. Instrum. Methods Phys. Res., Sect. A **694**, 133 (2012).

[27] E. Maclean, F. Carlier, M. Giovannozzi, T. Persson, and R. Tomás, Effect of linear coupling on nonlinear observables at the LHC, in *Proceedings of the 8th International Particle Accelerator Conference, IPAC-2017, Copenhagen, Denmark* (JACoW, Geneva, Switzerland, 2017), pp. 3151–3154, 10.18429/JACoW-IPAC2017-WEPIK092.

[28] L. R. Carver, X. Buffat, K. Li, E. Métral, and M. Schenk, Transverse beam instabilities in the presence of linear coupling in the Large Hadron Collider, Phys. Rev. Accel. Beams **21**, 044401 (2018).

[29] A. Franchi, E. Métral, and R. Tomás, Emittance sharing and exchange driven by linear betatron coupling in circular accelerators, Phys. Rev. ST Accel. Beams **10**, 064003 (2007).

[30] E. Métral, G. Hoffstaetter, and F. Willeke, Destabilising effect of linear coupling in the HERA proton ring, in *Proceedings of the 8th European Particle Accelerator Conference, Paris, France* (JACoW, Geneva, Switzerland, 2002).

[31] J. Jowett *et al.*, The 2018 Heavy-Ion Run of the LHC, in *Proceedings of the 10th International Particle Accelerator Conference, IPAC-2019, Melbourne, Australia* (JACoW, Geneva, Switzerland, 2019), 10.18429/JACoW-IPAC2019-WEYYPLM2.

[32] F. Carlier *et al.*, LHC run 2 optics commissioning experience in view of HL-LHC, in *Proceedings of the 10th International Particle Accelerator Conference, IPAC-2019, Melbourne, Australia* (JACoW, Geneva, Switzerland, 2019), pp. 508–511, 10.18429/JACoW-IPAC2019-MOPMP033.

[33] T. Persson, F. Carlier, J. Coello, J. Dilly, S. Fartoukh, E. Fol, A. Garcia-Tabares, M. Giovannozzi, M. Hofer, E. H. Maclean, L. Malina, P. K. Skowronski, M. L. Spitznagel,

R. Tomás, A. Wegscheider, and J. Wenninger, LHC optics corrections in run 2, in *Proceedings of the 9th LHC Operations Evian Workshop, Evian Les Bains, France* (CERN, Geneva, Switzerland, 2019).

[34] R. Tomás, O. Brüning, M. Giovannozzi, P. Hagen, M. Lamont, F. Schmidt, G. Vanbavinckhove, M. Aiba, R. Calaga, and R. Miyamoto, CERN Large Hadron Collider optics model, measurements, and corrections, Phys. Rev. ST Accel. Beams **13**, 121004 (2010).

[35] A. Bazzani, A. Pisent, and G. Turchetti, Normal forms for Hamiltonian maps and future applications to accelerators, CERN, Geneva, Technical Report No. CERN-SPS-87-38-AMS, 1987.

[36] A. Bazzani, P. Mazzanti, G. Servizi, and G. Turchetti, Normal forms for Hamiltonian maps and nonlinear effects in a LHC model, CERN Technical Report No. CERN-SPS-87-38-AMS, 1988.

[37] J. Bengtsson, Non-linear transverse dynamics for storage rings with applications to the low-energy antiproton ring (LEAR) at CERN, Ph.D. thesis, Lund University, 1988, 10.5170/CERN-1988-005.

[38] E. Forest, M. Berz, and J. Irwin, Normal form methods for complicated periodic systems: A complete solution using differential algebra and lie operators, Part. Accel. **24**, 91 (1989), https://cds.cern.ch/record/1053511.

[39] G. Turchetti, Beam stability analysis via normal forms and non perturbative methods, in *Non Linear Problems in Future Particle Accelerators* (World Scientific, Singapore, 1991).

[40] M. Berz, High-order computation and normal form analysis of repetitive systems, AIP Conf. Proc. **249**, 456 (1992).

[41] A. Bazzani, G. Servizi, E. Todesco, and G. Turchetti, A normal form approach to the theory of nonlinear betatronic motion, CERN, Geneva, CERN Yellow Reports: Monographs, 1994.

[42] E. Forest, *Beam Dynamics: A New Attitude and Framework, The Physics and Technology of Particle and Photon Beams* (Harwood Academic Publishers, Chur, Switzerland, 1998), Vol. 8, ISBN 978-90-5702-558-7.

[43] R. Bartolini and F. Schmidt, Normal form via tracking or beam data, Technical Report No. CERN-LHC-Project-Report-132, 1998.

[44] R. Tomas-García, Direct measurement of resonance driving terms in the Super Proton Synchrotron (SPS) of CERN using beam position monitors, Ph.D. thesis, University of Valencia, 2003, https://cds.cern.ch/record/615164.

[45] A. Franchi, Studies and measurements of linear coupling and nonlinearities in hadron circular accelerators, Ph.D. thesis, University of Frankfurt, 2006, https://d-nb.info/981264875/34.

[46] S. Fartoukh *et al.*, LHC configuration and operational scenario for run 3, CERN Technical Report No. CERN-ACC-2021-0007, 2021.

[47] G. Guignard, Betatron coupling and related impact of radiation, Phys. Rev. E **51**, 6104 (1995).

[48] D. A. Edwards and L. C. Teng, Parametrization of linear coupled motion in periodic systems, IEEE Trans. Nucl. Sci. **20**, 885 (1973).

[49] G. Ripken, Untersuchungen zur Strahlführung und Stabilität der Teilchenbewegung in Beschleunigern und Storage-Ringen unter strenger Berücksichtigung einer Kopplung der Betatronschwingungen, DESY, Technical Report DESY Internal Report No. R1-70/4, 1970.

[50] F. Willeke and G. Ripken, Methods of beam optics, AIP Conf. Proc. **184**, 758 (1989).

[51] I. Borchardt, E. Karantzoulis, H. Mais, and G. Ripken, Calculation of beam envelopes in storage rings and transport systems in the presence of transverse space charge effects and coupling, Z. Phys. C **39**, 339 (1988).

[52] V. A. Lebedev and S. A. Bogacz, Betatron motion with coupling of horizontal and vertical degrees of freedom, J. Instrum. **5**, P10010 (2010).

[53] C. Yunhai, Luminosity of asymmetric e^+e^- collider with coupling lattices, in *Proceedings of the European Particle Accelerator Conference, Vienna, 2000* (EPS, Geneva, 2000).

[54] W. Herr and B. Muratori, Concept of luminosity, in *Proceedings of CAS—CERN Accelerator School: Intermediate Accelerator Physics* (2006), pp. 361–378.

[55] S. Fartoukh *et al.*, First high-intensity beam tests with Telescopic Flat Optics at the LHC, CERN, Geneva, Technical Report No. CERN-ACC-2019-0052, 2019.

[56] O. S. Brüning, S. D. Fartoukh, M. Giovannozzi, and T. Risselada, Dynamic aperture studies for the LHC separation dipoles, CERN, Geneva, Technical Report No. CERN-LHC-Project-Note-349, 2004.

[57] H. Grote and F. C. Iselin, The MAD program, Technical Report No. CERN/SL/90-13 (AP), 2016.

[58] M. G. Minty and F. Zimmermann, Correction to: Measurement and control of charged particle beams, in *Measurement and Control of Charged Particle Beams* (Springer, Berlin, Heidelberg, 2003), pp. C1–C1.

[59] P. Thrane, R. Tomás, A. Koval, K. Ohmi, Y. Ohnishi, and A. Wegscheider, Measuring β^* in SuperKEKB with k modulation, Phys. Rev. Accel. Beams **23**, 012803 (2020).

[60] M. Hofer and R. Tomás, Effect of local linear coupling on linear and nonlinear observables in circular accelerators, Phys. Rev. Accel. Beams **23**, 094001.

[61] F. Carlier and R. Tomás, Accuracy and feasibility of the β^* measurement for LHC and high luminosity LHC using k modulation, Phys. Rev. Accel. Beams **20**, 011005 (2017).

[62] T. H. B. Persson, F. S. Carlier, M. Hofer, E. H. Maclean, R. Tomas Garcia, and A. Garcia-Tabares Valdivieso, MD4944: Local linear coupling measurement at the IPs, CERN Technical Report No. CERN-ACCNOTE-2020-0013, 2020.

[63] F. Soubelet, PYRWS, PYTHON Package to Prepare Rigid Waist Shift Operations in the CCC, GitHub repository, 10.5281/zenodo.6517668 (2022).

[64] M. Hostettler, R. D. Maria, T. H. B. Persson, A. Huschauer, D. Gamba, G. Roy, and M. S. Camillocci, Large Hadron Collider Optics Repository, 2022 Optics, GitLab repository (2022).

[65] R. Tomás, Optimizing the global coupling knobs for the LHC, CERN Technical Report No. CERN-ATS-Note-2012-019 MD, 2012.

[66] T. Persson, Transverse Coupling, OMC-OP Workshop, https://indico.cern.ch/event/828284/contributions/3467292/attachments/1921190/3178244/transverse_coupling_omc_op_v2.pdf.

[67] T. Persson, Stability of Linear Coupling in Run 2, https://indico.cern.ch/event/844692/contributions/3546747/attachments/1909102/3153959/coupling_stability.pdf.

[68] A. Wegscheider, A. Langner, R. Tomás, and A. Franchi, Analytical *n* beam position monitor method, Phys. Rev. Accel. Beams **20**, 111002 (2017).

[69] A. Abada *et al.*, FCC-ee: The lepton collider, Eur. Phys. J. Spec. Top. **228**, 261 (2019).

[70] A. Morita, H. Koiso, K. Ohmi, Y. Ohnishi, H. Sugimoto, and D. Zhou, Optics corrections including IP Local coupling at SuperKEKB, in *Proceedings of the 10th International Particle Accelerator Conference, IPAC-2019, Melbourne, Australia* (JACoW, Geneva, Switzerland, 2019), 10.18429/JACoW-eeFACT2018-TUOAB04.

[71] C. R. Harris, K. J. Millman, S. J. van der Walt, R. Gommers, P. Virtanen, D. Cournapeau, E. Wieser, J. Taylor, S. Berg, N. J. Smith, R. Kern, M. Picus, S. Hoyer, M. H. van Kerkwijk, M. Brett, A. Haldane, J. F. del R'ıo, M. Wiebe, P. Peterson, P. G'erard-Marchant *et al.*, Array programming with NumPy, Nature (London) **585**, 357 (2020).

[72] The pandas development team, pandas-dev/pandas: PANDAS (2020), https://pandas.pydata.org/about/citing.html.

[73] J. D. Hunter, MATPLOTLIB: A 2D graphics environment, Comput. Sci. Eng. **9**, 90 (2007).

[74] T. Gläßle, R. D. Maria, Y. Levinsen, and K. Fuchsberger, CPYMAD, 10.5281/zenodo.4724857 (2021).

[75] F. Soubelet, PyhDToolkit, An All-In-One Package for PYTHON Work in my Ph.D., GitHub repository, 10.5281/zenodo.4583205 (2020).

[76] L. Malina, J. Dilly, M. Hofer, F. Soubelet, A. Wegscheider, J. Maria Coello De Portugal - Martinez Vazquez, M. Le Garrec, T. Persson, J. Keintzel, H. Garcia Morales, and R. Tomás Garcia (OMC-Team), OMC3: PYTHON 3 Codes for Beam Optics Measurements and Corrections in Circular Particle Accelerators, GitHub repository, 10.5281/zenodo.7756297 (2020).

[77] J. Dilly, R. T. Garcia, and T. Persson (OMC-Team), Optics_functions, GitHub repository, 10.5281/zenodo.4518969 (2021).

[78] M. Hofer, J. Dilly, F. Soubelet, R. Tomás Garcia, and T. Persson (OMC-Team), PyLHC: Additional Tools for Particle Accelerator Data Analysis and Machine Information, GitHub repository, 10.5281/zenodo.7225904 (2020).

[79] D. Thain, T. Tannenbaum, and M. Livny, Distributed computing in practice: The Condor experience, Concurr. Comput. **17**, 323 (2005).